Euro-Mediterranean Journal for Environmental Integration
https://doi.org/10.1007/s41207-024-00480-9

ORIGINAL PAPER

The effect of erosion on hydraulic machine performance

Jamal EL Mansour[1] · **Patrick Hendrick**[2] · **Abdelowahed Hajjaji**[1] · **Fouad Belhora**[1]

Received: 17 June 2023 / Accepted: 31 January 2024

Abstract
Seawater pumped storage consists of pumping water from the sea to an upper reservoir to store electricity. The use of seawater as the fluid results in an erosion mechanism due to the presence of solid particles. In this paper, we study the effect of the fluid content on the performance of low-head pumps in the blade-to-blade section. The loss of blade thickness may cause damage due to the water pressure applied to the blade section. From our study, we conclude that the resulting erosion depends on the absolute velocity distribution whereas the thickness loss depends on the particle size, density, and velocity. For hydraulic pumps, erosion of the blades is more likely to occur at their trailing edge. A reduction of the blade orthogonal thickness to 10% results in flow deflection.

Keywords Seawater · Pumped storage · Erosion · Efficiency · Hydraulic machine

List of Symbols

U	Centrifugal velocity (m/s)
C	Absolute velocity (m/s)
C_u	Tangential velocity (m/s)—the tangential component of C
C_m	Meridional velocity (m/s)—the axial component of C
W	Relative velocity (m/s)—the velocity of the fluid due to the impeller rotation frame
$V_{erosion}$	Erosion velocity (m/s)
t	Blade thickness (m)
σ	Blockage ratio
γ	Slip factor
β	Blade angle (degrees)
η_H	Hydraulic efficiency (%)
α	Flow angle (degrees)
N_p	Particle number (considered to be 20 for all simulations)
V_p	Particle velocity (m/s)
r_p	Particle velocity (m)
d_p	Particle density (kg/m^3)
z	Number of runner blades
dS	Shroud diameter (mm)
CFD	Computational fluid dynamics
Re	Reynolds number
v_p	Vapor pressure
H_E	Effective head (m)

Indices

1	Entrance section (LE)
2	Outlet section (TE)
p	Particle
SW	Seawater
ss	Shroud suction section
sp	Shroud pressure side
s	Shroud
h	Hub
hs	Hub suction side
hp	Hub pressure side

Responsible Editor: Mohamed Ksibi.

✉ Jamal EL Mansour
elmansour.j@ucd.ac.ma

Patrick Hendrick
patrick.hendrick@ulb.be

Abdelowahed Hajjaji
hajjaji.a@ucd.ac.ma

Fouad Belhora
belhora.f@ucd.ac.ma

[1] LabSIPE Laboratory, National School of Applied Science, ENSA Chouaib Doukkali University, El Jadida, Morocco

[2] Aero Thermo Mechanique, Université Libre de Bruxelles, Avenue Franklin Roosevelt 50, Brussels, Belgium

Published online: 25 April 2024

Introduction

Pumped storage (PSS) is a process used to store excess electricity by using the vertical difference between two water reservoirs separated by a given altitude. According to the International Hydropower Association, pumped storage is considered to be the largest battery for renewable energy systems, with about 94% of the total stored capacity. Owing to the intermittency of solar and wind, the development of pumped storage by using rivers or dams will improve grid quality by managing production and the electricity demand.

An alternative to PSS is seawater pumped storage. This new technology uses the sea as a lower reservoir. The first such project was located in Okinawa (Japan) with an installed capacity (rated power) of 150 MW (Fig. 1). This project has one penstock and one production room. The sea is 150 m below the water level of the upper reservoir. The seawater flow was 120 m^3/s (Hashimoto 1986).

The advantage of using the sea is to reduce the cost of construction of the lower reservoir and benefit from its unlimited capacity. Seawater can work with a pump turbine or separated pump and turbine with a penstock to carry water under high pressure between the two dams. The Francis turbine is a rotating machine with blades and inlet guide vanes, whereas an impulse turbine consists of a rotating runner with buckets. The Francis turbine can be used as a pump or as a turbine by switching the rotational direction. The fatigue of this machine results from the water hammer effect when switching from pump to turbine mode. In this work, we study the effect of erosion on the hydraulic machine for low-head applications.

Seawater contains 35 g per liter of salt. This high concentration of NaCl means that the fluid corrodes the material used for the blades. It is in contact with rocks, which generate solid particles in the fluid content. These particles cause an erosion mechanism on the turbine or pump owing to the passage of the fluid in the blade-to-blade section.

Seawater is especially used for fisheries and small desalination units. In Morocco, several small cities have large capabilities for fishing. The use of seawater reservoirs with low-height pumps can help communities to develop their fishing production.

The present paper discusses the erosion of a hydraulic pump with 3 kg/s and a height of 5 m. It was concluded that the erosion mainly depends on the size of the particles, the density, and the velocity distribution. The inlet of the pump is likely to be impacted by cavitation, whereas erosion occurs at the leading edge of the blade.

The geometry was generated by the commercial software CFTurbo and simulated by Simerics. CFTurbo is an interactive design software for turbomachinery. The user defines inputs such as the fluid flow, height, and rotational speed. The generated geometry can be modified by changing the blade angles, blade thickness, and height. Simerics is a CFD software with three modules: flow, cavitation, and particle.

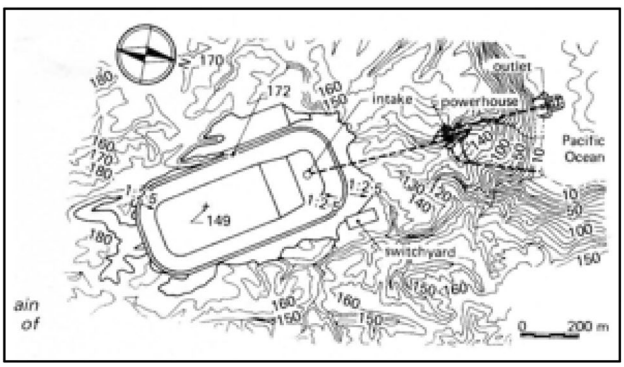

Fig. 1 Okinawa seawater pumped storage schema and elevation data (Hashimoto 1986)

Literature review

Hydraulic turbines transfer the kinetic energy of the fluid into mechanical power by using a mechanical rotating device, which is the runner. The fluid motion and its contact with the walls will result in material mass loss (Sangal et al. 2018). The mass loss depends on the salinity of the water (corrosion) and the presence of solid particles (erosion). In addition, the fluid moving from the inlet to the outlet is subject to a pressure gradient due to the curvature of the blade. This pressure gradient increases from the inlet to the outlet (for the pump) but decreases in the case of a turbine. A low static pressure at the inlet can be a source of cavitation, which is related to the Net Positive Suction Head (NPSH) of the pump (Noon 2021). In a turbulent flow analysis, the viscosity of the fluid is an internal property of the fluid. Owing to the turbulence intensity, the eddy viscosity appears, resulting in divergence of the velocity in the near field. This is the case of the CFD model (k–w), where the unknowns in the Navier–Stokes equations are solved by using the divergence of the viscosity and the density for the main equation of the flow velocity (Ayancik 2014).

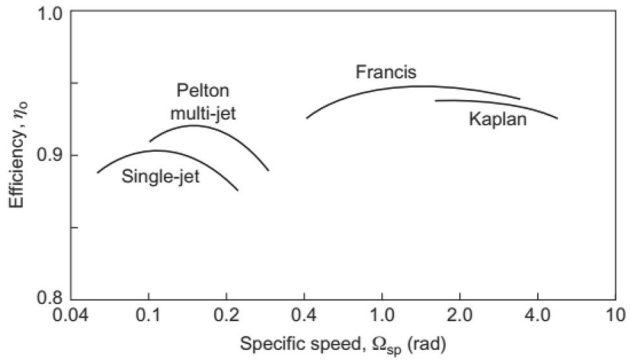

Fig. 2 The variation of the hydraulic turbine efficiencies with specific speed (radians) (Dixon et al. 2014)

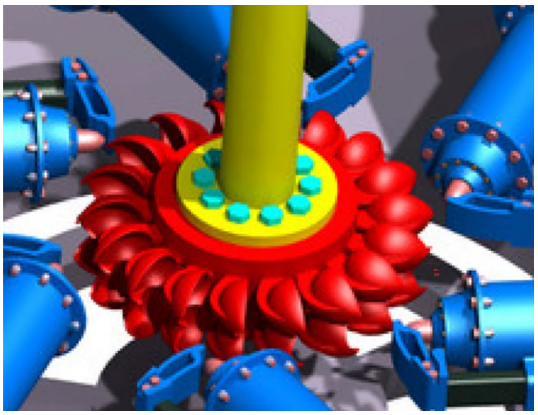

Fig. 3 A vertical Pelton turbine rotor with six jet nozzles

Hydraulic turbines

Hydraulic machines are used to convert hydraulic energy to mechanical shaft power, which is coupled to a generator. The available power depends on the hydraulic efficiency, water flow, altitude, and turbine efficiency. The efficiency of the hydraulic turbines depends on the specific speed, which is defined as

$$N_s = \frac{N\sqrt{Q}}{H^{\frac{5}{4}}}. \tag{1}$$

Figure 2 shows the variation in the efficiency with specific speed (in radians). The radial (Francis) turbine has an interval from 0.4 to 1.1, with good efficiency due to the use of radial blades and inlet guide vanes (IGVs). The use of IGVs controls the load by adjusting the outlet blade angle.

The hydraulic efficiency is defined as

$$\eta_{\mathrm{H}} = \frac{\text{mechanical output power}}{\text{inlet kinetic energy}}. \tag{2}$$

The impulse (Pelton) turbine is usually used for a low specific speed with an optimum Ns of 0.15. This is because the Pelton turbine is used for high altitudes (up to 900 m).

Impulse turbine

A Pelton turbine consists of water jet nozzles that run under high pressure and absolute velocity (Fig. 3).

The runner is constituted by a wheel and buckets. The water jet comes from a nozzle with a high velocity ratio. The optimum jet velocity ratio $\frac{U}{C_1}$ is 0.5 (Fig. 3), depending on the ratio of the relative velocities $\frac{W_2}{W_1}$. For the impulse turbine, the relative velocity ratio is about 0.8. As the fluid directly attacks the buckets in the horizontal plane, the tangential velocity of the absolute velocity is equal to zero and C_1 at the inlet is equal to the sum of the relative velocity and the peripheral velocity:

$$C_1 = W_1 + U, \tag{3}$$

where

$$U_1 = U_2 = U = \pi dw. \tag{4}$$

At the outlet, the flow leaves the buckets with an angle β_2. Thus, the absolute velocity at the outlet will be

$$C_2 = W_2 + U. \tag{5}$$

By using Eq. (2), the power delivered by the turbine is obtained as

$$P = U_1 C_{u1} - U_2 C_{u2} = U\left(C_{u1} - C_{u2}\right). \tag{6}$$

The hydraulic efficiency of the impulse turbine is defined as

$$\eta_H = \frac{P}{\frac{C_1^{\,2}}{2}} = \frac{U\left(C_{u1} - C_{u2}\right)}{\frac{C_1^{\,2}}{2}}. \tag{7}$$

The triangle velocity at the outlet shows that the tangential component is related to the outlet blade angle. One can conclude that

$$C_{u2} = U - W_2 \cos\beta_2. \tag{8}$$

By substituting C_{u2} of Eq. 6 into Eq. 4, we obtain

$$P = U(C_{u1} - U + W_2\cos\beta_2) = U(W_1 + W_2\cos\beta_2), \tag{9}$$

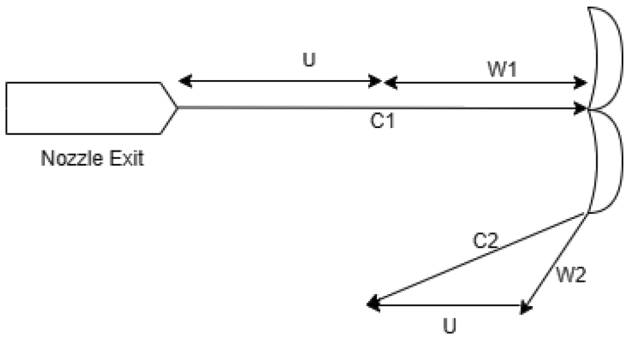

Fig. 4 Velocity diagram of an impulse (Pelton) turbine

$$P = UW_1(1 + k\cos\beta_2), \tag{10}$$

where

$$k = \frac{W_2}{W_1}, \tag{11}$$

$$P = U(C_1 - U)(1 + k\cos\beta_2). \tag{12}$$

Then, the hydraulic efficiency will be

$$\eta_H = 2\vartheta(1 - \vartheta)\left(1 + k\cos\beta_2\right). \tag{13}$$

The variation of the hydraulic efficiency with the jet velocity ratio shows a maximum at 0.5 (Figs. 4, 5).

The jet velocity should be kept at twice the peripheral velocity. However, as there are no radial blades, the absolute velocity should be high to rotate the runner efficiently. The weakness of the impulse turbine is its partial load operation, as the jet velocity depends on the inlet velocity of the flow that comes through the penstock. Reducing the jet velocity may result in flow leakage losses between the jet outlet and the impeller buckets because part of the flow will be lost. Owing to the high jet velocity, the erosion rate is more important at the jet nozzle (Padhy and Saini 2011).

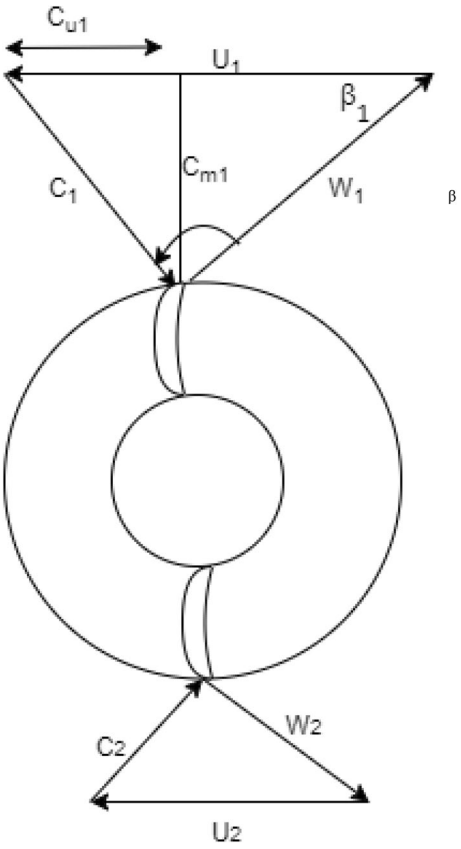

Fig. 6 Velocity diagram of a Francis turbine runner at the inlet and outlet

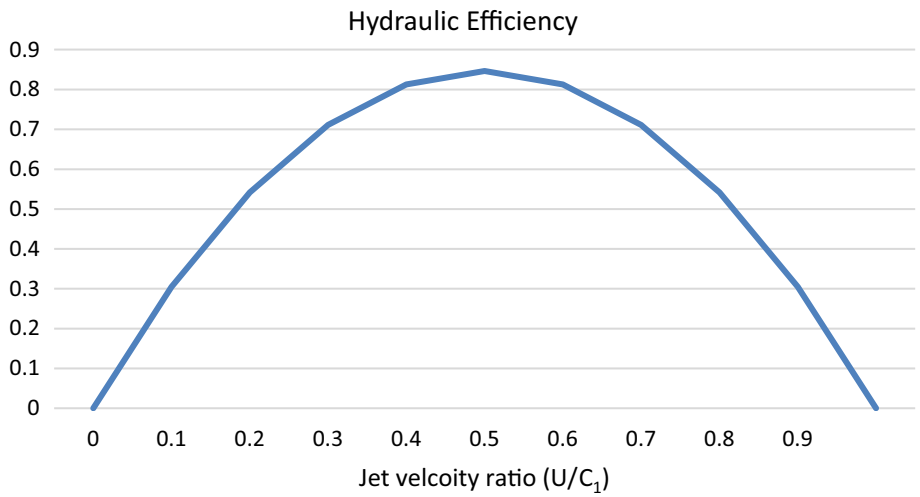

Fig. 5 Variation of the hydraulic efficiency of an impulse turbine with the jet velocity ratio

Fig. 7 Variation of the relative velocity for a Francis turbine runner

Reaction turbine

Reaction machines use blades to increase or decrease the pressure. The curvature of the blade changes the pressure distribution because the fluid follows the blade profile. Flow along a curved profile is always accompanied by a pressure gradient (Gülich 2014)

$$\frac{\mathrm{d}p}{\mathrm{d}r} = \rho\frac{C^2}{r}. \tag{14}$$

The blade geometry (Fig. 6) is generated by a Bézier curve by selecting a control point and the calculation of the Bernstein polynomial coefficients (Aungier 2000). The fluid hydraulic energy is transferred to the rotor by the rotation of the blade. The turbine power is correlated with the given machine torque, which depends on the difference of the tangential velocities at the inlet and outlet section:

$$P = U_1C_{u1} - U_2C_{u2}. \tag{15}$$

In the case of radial machines, additional energy is added as U_1, which is different from U_2. The total energy is constituted by gravitational energy and kinetic energy. If the design considers no swirl at the outlet, then $C_{u2}=0$. The power output is linked to the inlet conditions.

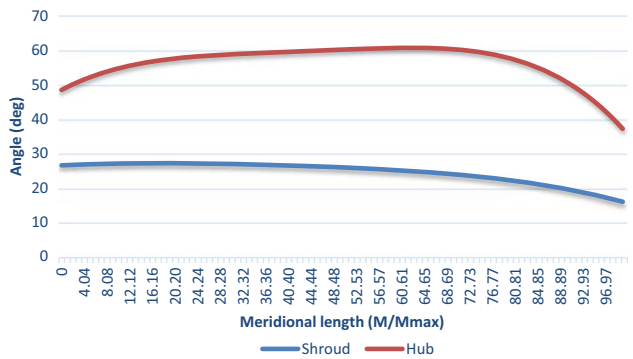

Fig. 8 Blade angle distribution at the FT runner

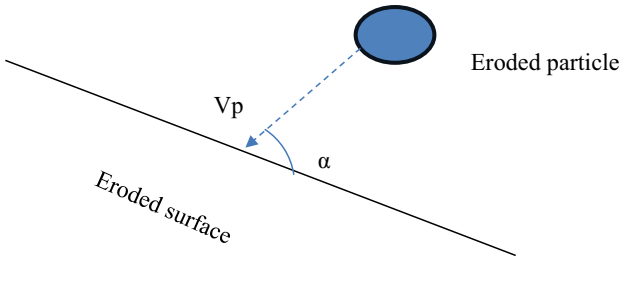

Fig. 9 Erosion mechanism

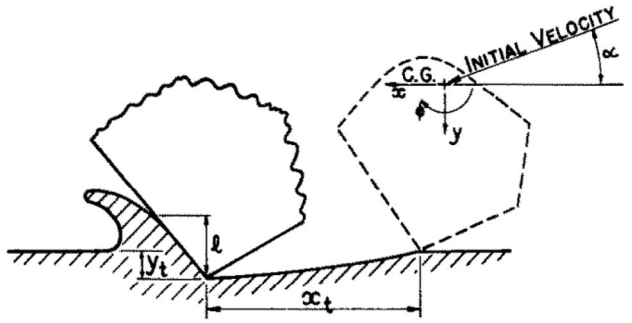

Fig. 10 Abrasion due to a particle attack with wall contact (Finnie 1960)

Equation (12) yields

$$P = U_1C_{u1}. \tag{16}$$

From the inlet triangle velocity (Fig. 6)::

$$C_{u1} = U_1 + W_1\cos\beta_1. \tag{17}$$

Then, Eq. (13) becomes

$$P = {U_1}^2 + U_1W_1\cos\beta_1, \tag{18}$$

or

$${C_1}^2 = {W_1}^2 + {U_1}^2 + 2U_1W_1\cos\beta_1. \tag{19}$$

Then, from Eq. (15), we have

$$P = {U_1}^2 + \frac{{C_1}^2 - {W_1}^2 - {U_1}^2}{2} = \frac{{U_1}^2 - {W_1}^2 + {C_1}^2}{2}. \tag{20}$$

One should consider that the ratio $\frac{W_2}{W_1}$ should be at least 1. In case of swirl, Eq. (17) becomes

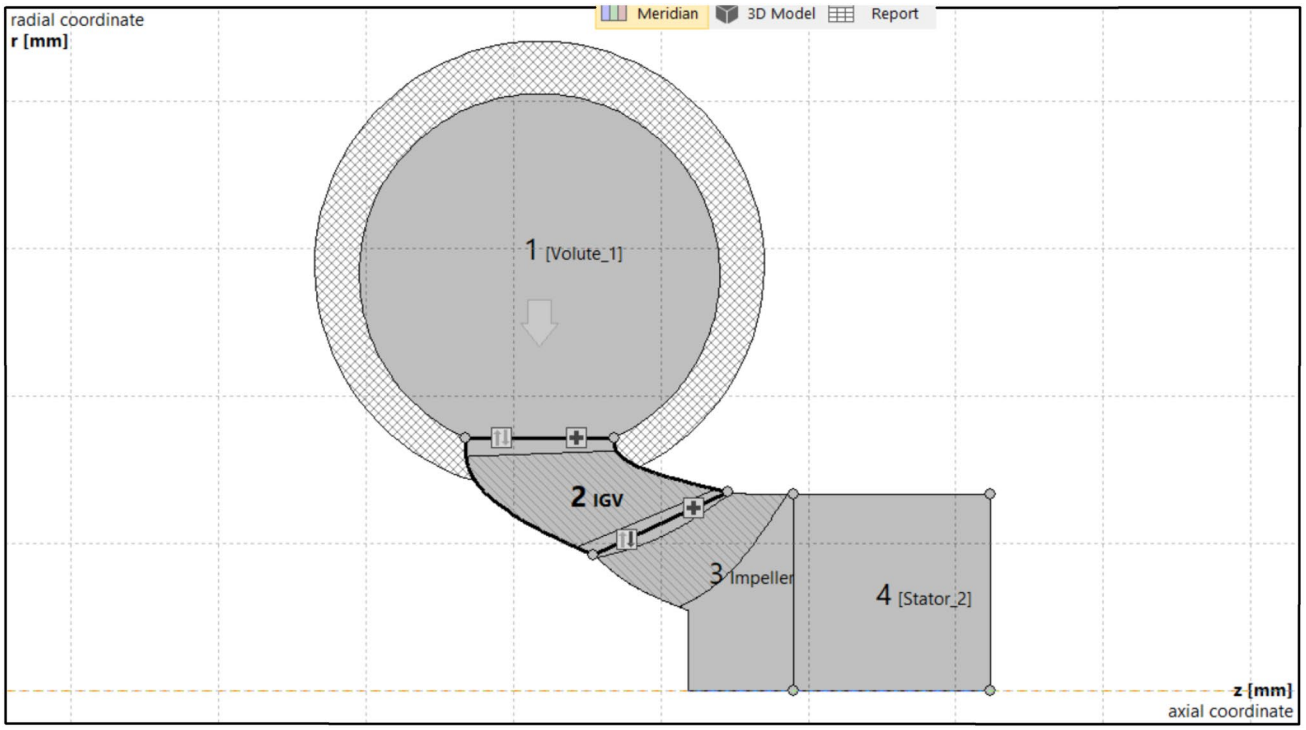

Fig. 11 The meridional contour of the FT design by CFTurbo

Table 1 Constant values of thickness distribution for small pump impeller diameter (less than 600 mm)

Trailing edge section	Leading edge section
$A_0 = 5.479539 \times 10^{-2}$	$A_0 = 4.703753 \times 10^{-2}$
$A_1 = -1.7782618 \times 10^{-4}$	$A_1 = -1.503196 \times 10^{-4}$
$A_2 = 2.046219 \times 10^{-7}$	$A_2 = 1.706213 \times 10^{-7}$

$$P = \frac{(U_1{}^2 - U_2{}^2) - (W_1{}^2 - W_2{}^2) + (C_1{}^2 - C_2{}^2)}{2}. \tag{21}$$

The relative component of the velocity does not contribute to the increase of the output power; thus, it should be controlled. For a Francis turbine runner, the inputs are

$$P_{\text{in}} = 7\,\text{bar}; H_{\text{g}} = 60\text{m}; Q = 1.53\text{E}5\frac{\text{m}^3}{\text{h}}.$$

The variation of the relative velocity obtained by using CFTurbo software is shown in Fig. 7.

The velocity increases from the inlet to the outlet, while the absolute velocity is decreased from the IGV outlet to the runner outlet. However, decreasing the static pressure is accompanied by an increase of the relative velocity. From Gülich (2014), for boundary layer conditions, the relative velocity is considered to be equal to 0 at the wall, which means that the particles will follow the flow given by the absolute velocity.

As

$$\vec{W}_{2ss} = \vec{C2}_{ss} - \vec{U}_{2s} \tag{22}$$

and owing to the distribution of the blade angles, the ratio $\frac{W_{2ss}}{W_{1s}}$ should be superior to the ratio $\frac{W_{2hs}}{W_{1h}}$ (Fig. 8).

As the radius at the outlet is increased, this means $U_2 > U_1$. In Eq. (19), the value of W is affected by two parameters, viz. the outlet radius and the blade angle.

The degree of reaction is defined as the ratio of the fluid energy transferred to the rotor divided by the total energy available during the passage of the fluid through the runner. It defines how much the runner contributes to the pressure decreases compared with the IGV.

In the blade geometry design strategy, we define two blade thickness modes that depend on solid trimming: the orthogonal thickness and tangential thickness. The thickness is defined as how blade thickness is added on both sides of the blades.

Table 2 Erosion models for a hydraulic Francis turbine

Model	Equation
Finnie	$E_r = kV_p{}^2 f(\alpha)$ α: angle of attack (°) V_p: particle velocity (m/s) K: a material constant described later in the text
IEC62364	$S = W^3 \times k_m \times k_f \times PL$ PL: particle loading S: abrasion depth (mm/year) $\mathrm{PL} = \int C(t) k_{\mathrm{size}}(t) k_{\mathrm{shape}}(t) k_{\mathrm{hardness}}(t) \mathrm{d}t$ K_m: metal coefficient that characterizes the resistance of the metal to abrasion K_f: a factor that characterizes the effect of turbulence on the abrasion mechanism W: the velocity component given by: $W_{\mathrm{guide\_vanes}} = 0.55\sqrt{2gH_E}$ $W_{\mathrm{runner}} = \left(0.25 + 0.33 n_s\right)\sqrt{2gH_E}$ where n_s is the specific speed C: particle concentration
Bajracharya	$E_r = a(\mathrm{size})^b$ Where a and b are constants that depend on the particle concentration
Thapa	$E_r = 6E - 5y^{3.13}$ E: Young's modulus y: the particle velocity at a 45° angle E_r: the erosion in mg per kg of eroded material

The orthogonal thickness (t) consists of adding thickness to the normal surface of the blade sections, while the tangential thickness means adding thickness in the direction tangential to the surface.

$$\text{Tengential thickness} = \frac{t}{\sin\beta}. \tag{23}$$

Along the blade, the thickness value is constant. For a small pump runner, the ratio $\frac{t}{d}$ is defined by the empirical equations developed by Schwanse (1990): for stainless steel and an outlet diameter d_2 between 100 and 600 mm, we have

$$\frac{t}{d_2} = A_0 + A_1 d_2 + A_2 {d_2}^2. \tag{24}$$

Table 3 Francis turbine design inputs

Parameter	Value
Inlet pressure	1.013 bar
Seawater flow	70 m^3/s
Head	70 (m)
Seawater vapor pressure (20°)	0.022 bar
Kinematic viscosity of seawater	9.37×10^{-7} m^2/s at $P = 1.013$ bar

In a rotating machine, the diameter of the impeller is related to the peripheral velocity. For the same U, decreasing the radius results in increasing the rotational speed, which means increasing the blade thickness to resist the pressure forces. For CFTurbo, the thickness values for the radial impeller is constant under a certain value.

The blade blockage, which is how the thickness blocks the passage of the flow in the blade-to-blade section, depends directly on the orthogonal thickness as

$$\sigma = \frac{t_1}{t_1 - \frac{2\pi r_1}{z}}. \tag{25}$$

At the inlet section, the meridional velocity depends on the flow passage area

$$C_{m1} = \frac{Q_1}{2\pi r_1 b_1}. \tag{26}$$

When the flow passes the blade, the meridional velocity is increased owing to the blade blockage:

$$C_{m\prime} = C_{m1}\sigma. \tag{27}$$

From the inlet velocity triangle, we have

$${W_1}^2 = {C_{m1}}^2 + {W_u}^2 = {C_{m1}}^2 + {W_1}^2(\cos\beta_1)^2, \tag{28}$$

$${W_1}^2 = \frac{{C_{m1}}^2}{\sqrt{1 - (\cos\beta_1)^2}}. \tag{29}$$

From Eq. (20), one can estimate the distribution of the blade thickness from the hub to shroud and from the inlet to the outlet. Fixing the value of σ, we can estimate the blade thickness for a given radius.

Table 4 Parameters used for CFD simulations in Simerics

Parameter	Value
r	100 µm
Ψ	0.1
K	2
p	1200 MPa
Material	13Cr-4Ni stainless steel (Thapa, 2015)
Particle mass	2.1×10^{-10} kg ($r = 100$ µm)
k	8.7×10^{-23}
Particle density	50 (kg/m^3)
Relaxation time	1.24 s
Stokes number	0.0012

Table 5 Blade height design parameters

Design strategy	Ratio value
High ratio	$\frac{b_1}{dS_1} = 0.35$
Design point	$\frac{b_1}{dS_1} = 0.339$
Low ratio	$\frac{b_1}{dS_1} = 0.3$

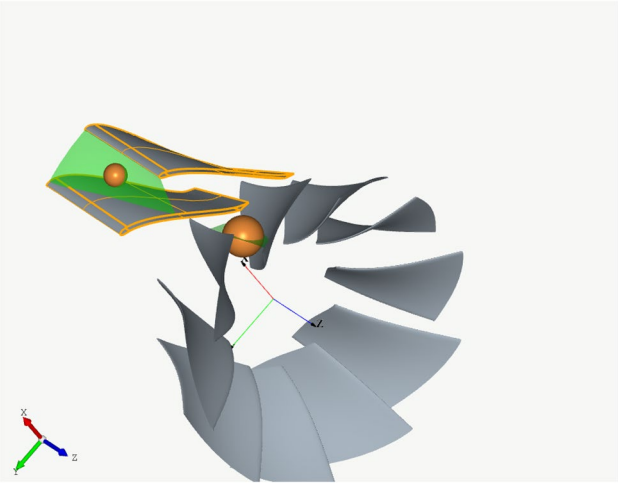

Fig. 12 The 3D geometry of the Francis turbine and the flow passage area in the IGV

The flow deflection or separation is directly linked to the thickness loss by the blockage ratio and slip factor. The flow is supposed to be guided perfectly by the blade wall in the case of an infinite number of blades, thus

$$C_{u2\infty} - C_{u2} = (1-\gamma)U_2, \tag{30}$$

$$\gamma = 1 + \frac{C_{u2}}{U_2} - \frac{C_{u2\infty}}{U_2}. \tag{31}$$

From the outlet triangle velocity,

$$\tan\beta_2 = \frac{C_{m2}}{U_2 - C_{u2\infty}}. \tag{32}$$

Thus,

$$\gamma = \frac{C_{u2}}{U_2} + \frac{C_{m2}\sigma}{U_2 tan\beta_2}. \tag{33}$$

The slip factor depends on the outlet blade angle, blockage ratio, and axial component of the absolute velocity. A very low value of the slip factor means flow separation (Gülich 2014).

Erosion

Erosion is considered to describe the loss of material mass when exposed to attack by solid particles. In general, the erosion rate depends on the particle size (S), particle velocity (V_p), and impingement angle (α) (Bardal 1985) (Fig. 9):

$$E_r = f(S, V_p, \alpha). \tag{34}$$

Some empirical models exist in literature and can be applied to hydraulic turbines (Gautam et al. 2020; Thapa and Dahlaug 2012; Koirala 2016) (Figs. 10, 11; Table 1).

The particle trajectory depends on the drag forces between the fluid and the solid particle. The equation of conservation of energy for the particle is

$$D_{\text{forces}} = m_p \frac{dV_p}{dt}, \tag{35}$$

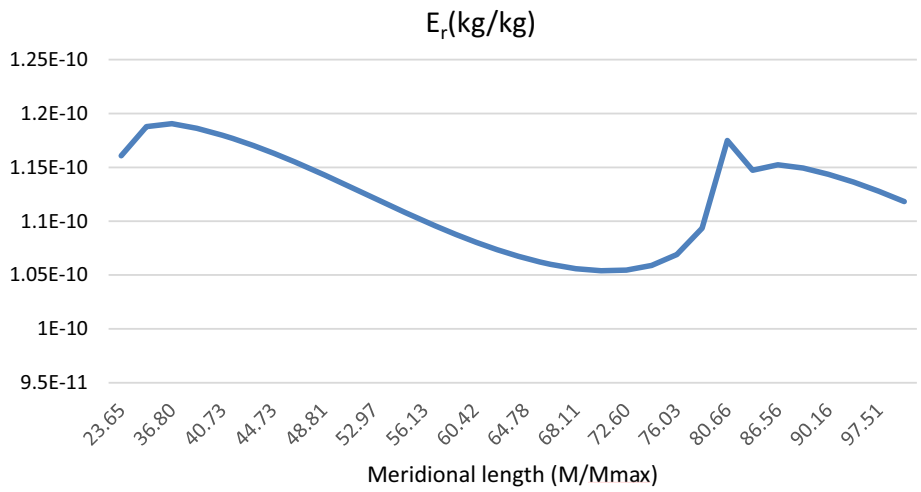

Fig. 13 The erosion rate for a Francis runner turbine

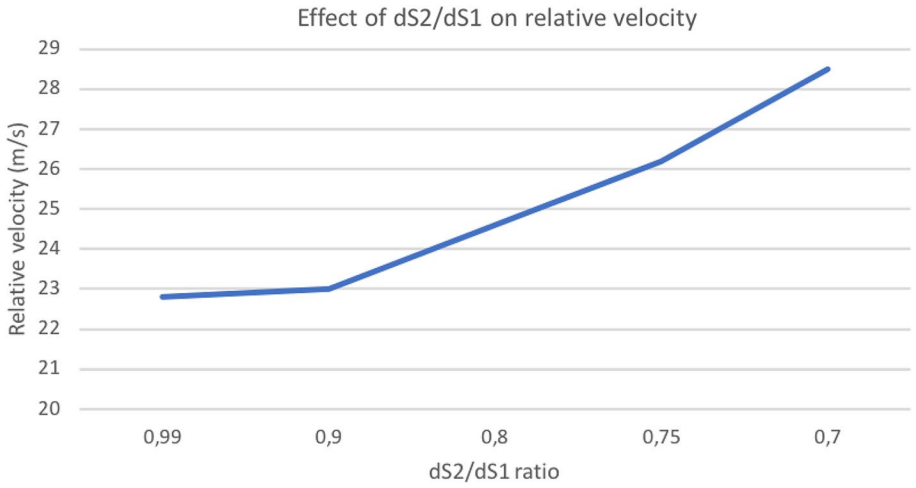

Fig. 14 The effect of the outlet diameter on the relative velocity at the exit

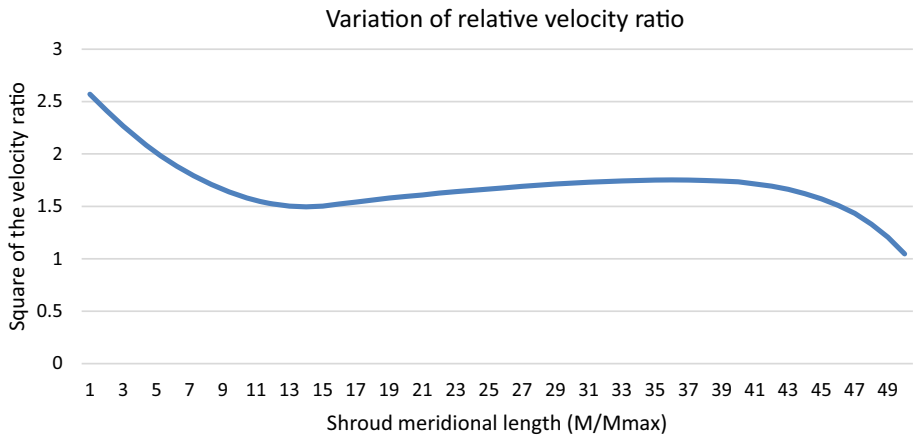

Fig. 15 The effect of the outlet diameter on the erosion ratio

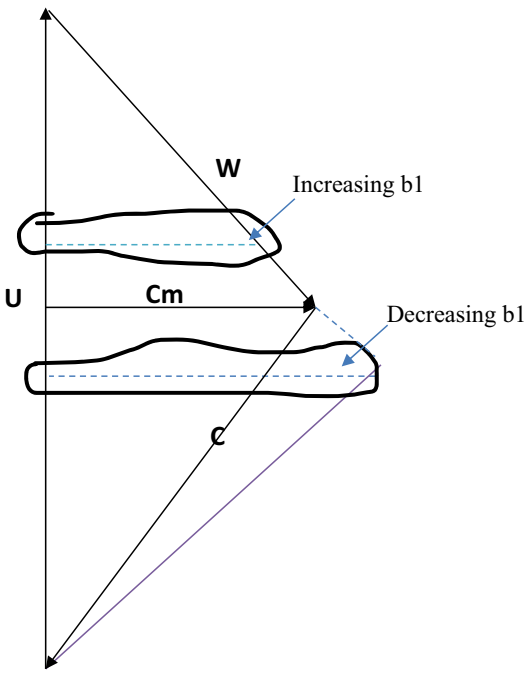

Fig. 16 The effect of b_1 on the velocity triangle

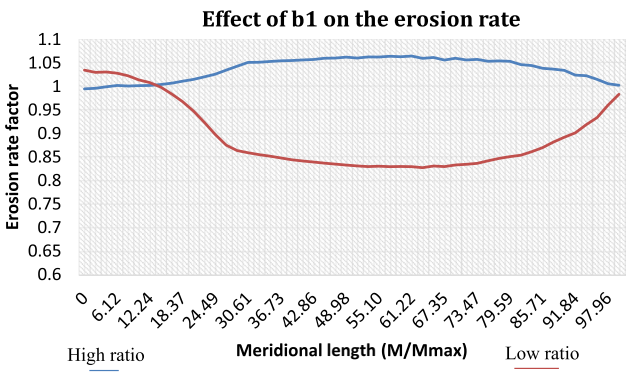

Fig. 17 The effect of b_1 on the relative velocity distribution from the LE to TE for the FT runner

$$\text{where} D_{\text{forces}} = C_D \pi \frac{{r_p}^2}{2} \left(V_p - C\right)^2, \tag{36}$$

$$\text{And} m_p = \frac{4}{3} \pi {r_p}^3 \rho_p. \tag{37}$$

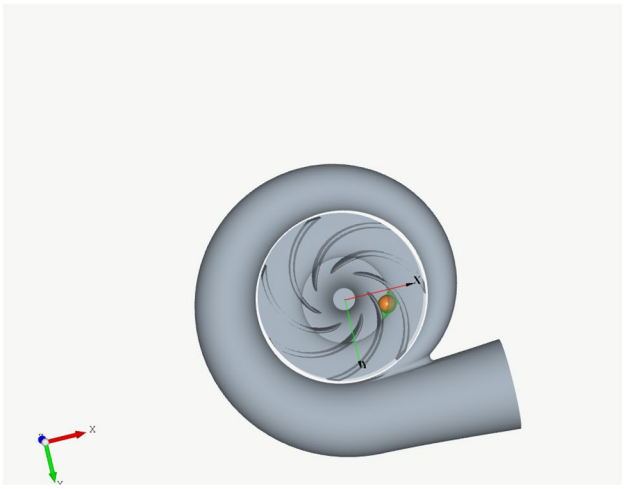

Fig. 18 The 3D geometry of the radial pump

C_D is the drag force coefficient, which depends on the Reynolds number of the particle trajectory. According to Messa et al. (2019),

$$C_D = \begin{cases} \frac{24}{Re_p}(1 + 0.15Re_p^{0.687}), Re_p < 1000 \\ 0.44, otherwise \end{cases}. \quad (38)$$

The initial value of the particle velocity was chosen as equal to the water's absolute velocity, owing to the high density of the fluid. The particle velocity distribution will fix the particle trajectory according to Lagrangian theory (Eq. 32). The angle coefficient depends on the material type. For turbine manufacturing, the usual material used is 16Cr-5Ni (Thapa and Dahlaug 2012), which is a ductile material (Table 2).

For turbomachinery applications, the distribution of the relative velocity alongside the blades depends on the blade and flow angle, which impact the particle impingement angle of the solid particles. From the above table, the Finnie model is most appropriate as it assumes that the erosion depends on the particle trajectory and boundary conditions. The flow angle coefficient is distributed as

$$f(\alpha) = \begin{cases} \frac{1}{3}(\cos\alpha)^2, \alpha > 18\text{deg} \\ \sin 2\alpha - 3(\sin\alpha)^2, \alpha \leq 18deg \end{cases}. \quad (39)$$

The constant k in the Finnie equation depends on the material and particle properties:

$$k = \frac{m}{p\Psi Y}, \quad (40)$$

where M is the particle mass, Y is the ratio of the horizontal forces divided by the vertical forces, and Ψ is the abrasion depth, which depends on the material properties as

$$\Psi = \frac{1}{y_t}.$$

For this simulation, the parameter k is defined as the Vickers hardness index. This index is an intrinsic material

Table 6 Input data for the hydraulic pumps

Parameter	Value
Head	5 m
Volumetric flow	12 m^3/s
Rotational speed	3000 rpm
Wall function	Bounce
Effect of gravity	Yes, in the direction of the flow
Time order	First order
Numerical solution	Upwind
Linear solver	Conjugate gradient squared (CGS)

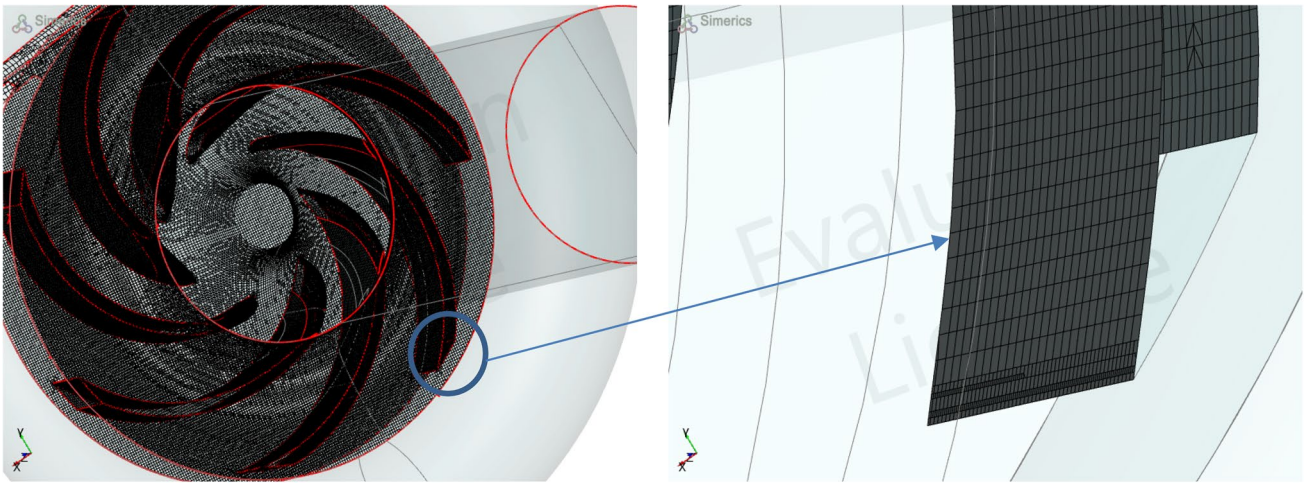

Fig. 19 The meshing quality

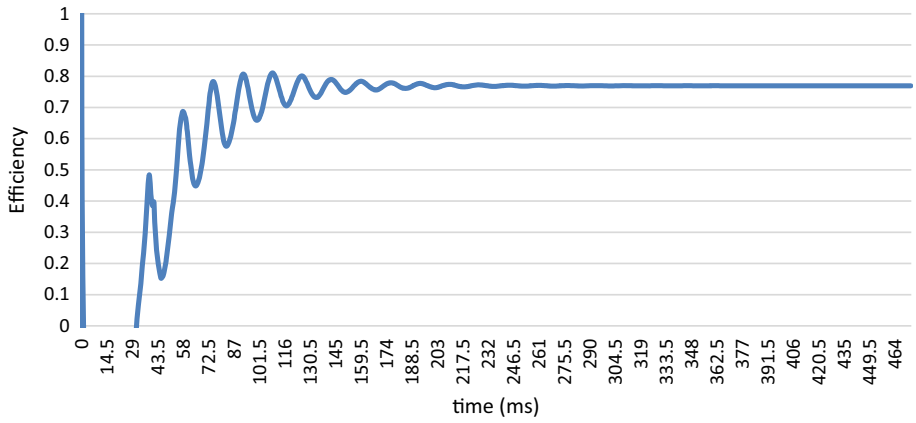

Fig. 20 The pump efficiency response

property that defines the resistance of the wall material to triangle solid particles. It is the high-pressure force applied by a particle surface to the wall.

Research results

Francis turbine

For the simulation, we chose one set of characteristics from the input data (Table 3).

The geometry was generated by using CFTurbo software. This software is an interactive tool to design radial machines. The design mode is an automated design. The geometry of the FT consists of the volute, IGV (stator), runner, outlet stator (for CFD simulation), and volute extension (flow analysis).

The 3D geometry is shown in Fig. 12.

Seawater exhibits a lower vapor pressure at the same thermodynamic point in comparison with water, which reduces the cavitation or vapor mass fraction. Cavitation is measured by the calculation of the NPSH and the Thomas coefficient.

$$\sigma = \frac{H_S}{H_E} = \frac{\left(\frac{p_v - p}{\rho g} - z\right)}{H_E}. \tag{41}$$

The calculation inputs are summarized in Fig. 13 and Table 4.

The erosion rate is much more important at the inlet section, where the absolute velocity is high. The loss of thickness depends on the exposure time.

$$t_l = \mathrm{ER}\left(\frac{\mathrm{kg}}{\mathrm{m^2 s}}\right) \times \frac{\mathrm{time}}{\rho_m}. \tag{42}$$

In case of increasing the outlet runner diameter, the peripheral velocity increases while the relative velocity decreases. Increasing the value of the ratio $\frac{dS_2}{dS_1}$ from 0.9 to 0.99 results in a decrease in the relative velocity W_2 (Fig. 14).

As the erosion rate is dependent on the velocity distribution, the deviation of the erosion rate factor from the design point is

$$E_r(\mathrm{factor}) = \frac{E_r(\mathrm{newdesign})}{E_r(\mathrm{designpoint})} \alpha(\mathrm{velocityratio})^2. \tag{43}$$

Increasing the outlet diameter by 10% may decrease the erosion rate by a factor of 2.5.

The inlet blade height has an impact on the hub to shroud velocity distribution. Increasing the blade height means decreasing the meridional velocity (Fig. 15).

Table 5 summarizes the input data for the impeller design.

Two design cases were investigated, with a high or low ratio $\frac{b_1}{dS_1}$. Figure 16 shows the variation of the relative velocity with the meridional length from the inlet (LE) to outlet (TE) section.

Reducing the inlet blade height will result in an increase in the absolute velocity, which means an increase in the particle velocity (Fig. 17).

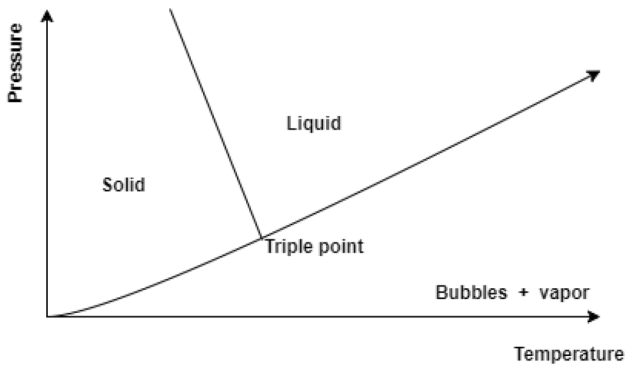

Fig. 21 Water phase diagram

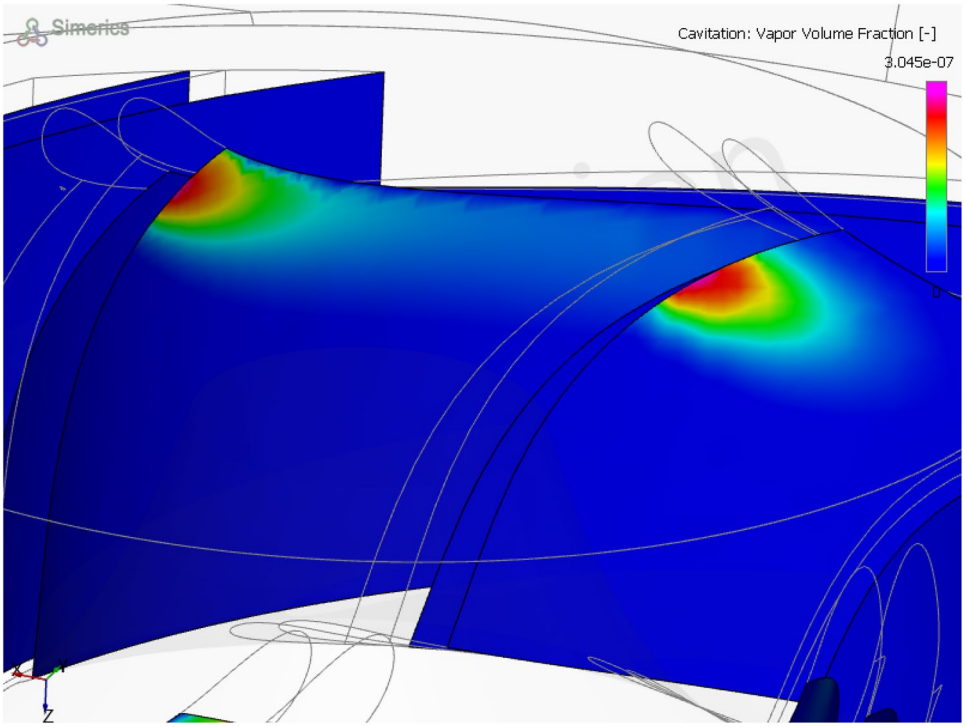

Fig. 22 Cavitation of the pump

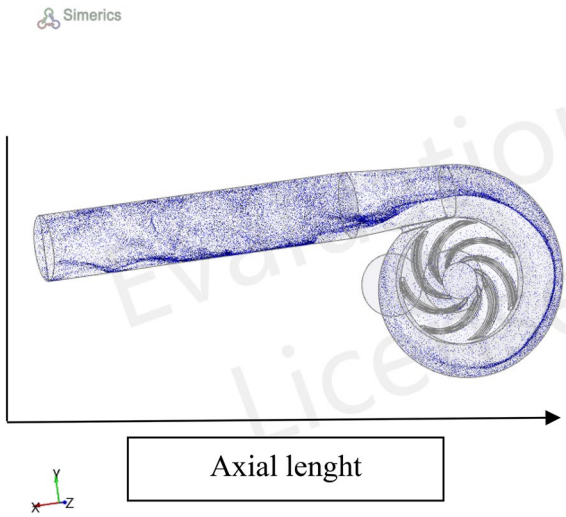

Fig. 23 Particle trajectory in the impeller and volute section

Hydraulic pump

For the CFD simulation, three modules in the commercial software Simerics were used: flow analysis, turbulence, and erosion. For our case, we did an analysis for a small hydraulic pump that can be used to pump seawater with very low altitude. This application is mostly used for places where seawater is used for fisheries (Fig. 18).

The input data are summarized in Table 6.

The simulations solved the Navier–Stokes equations with the *k*–*w* turbulence model, which is a mass conservation problem. The CGS solver is used for the numerical solution (Fig. 19).

The geometry of the pump impeller is shown in Fig. 18:

For Simerics, the automated binary meshing is used to generate the mesh, which consists of the critical edge angle and the curvature resolution.

A transient simulation was selected for the erosion process. The time response of the pump is shown in the Fig. 20.

At the inlet section of the pump, the pressure is very low, which can result in cavitation phenomena. However, the role of the pump is to conduct the fluid through a given height by initially increasing its velocity, which is associated with a pressure decrease.

For water, at the inlet atmospheric conditions, with a pressure drop beyond a certain value, the fluid can exist in liquid, vapor, or gas phase (Fig. 21), leading in this case to the cavitation phenomena. At the pump inlet, the pressure is reduced to increase the velocity, which results in vaporization of water. This situation is associated with the appearance of bubbles. The presence of vapor and gas

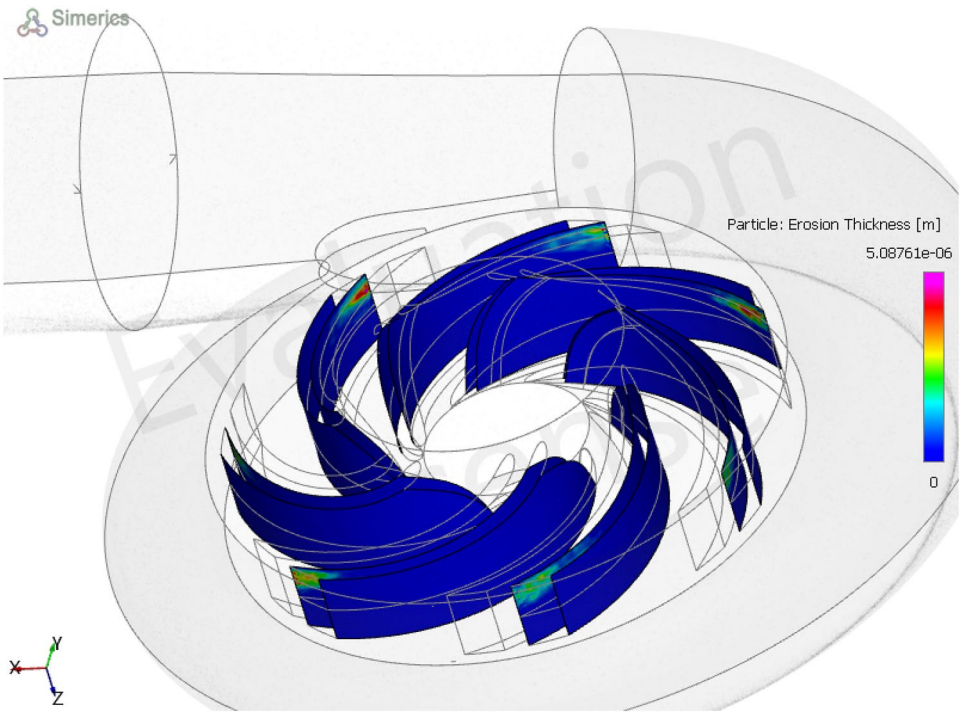

Fig. 24 Erosion thickness for the pump

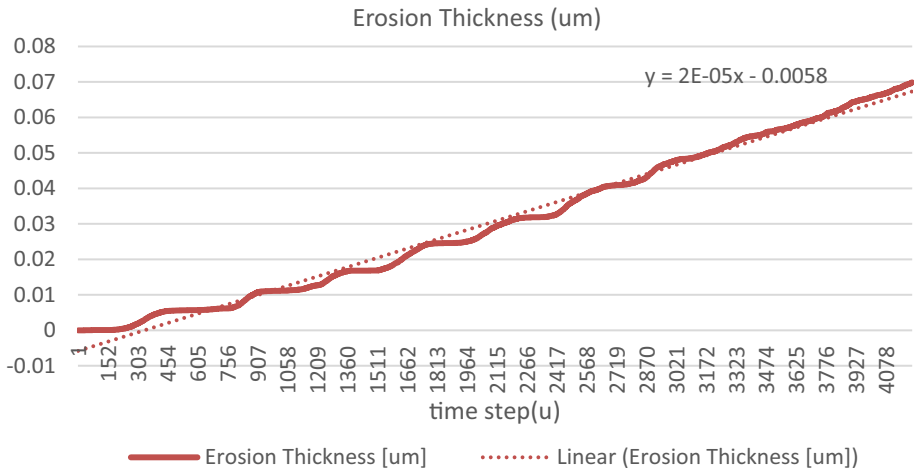

Fig. 25 Variation of the erosion thickness in the blade-to-blade section with time (releasing mode: every time step)

cause pressure oscillations on the blades. The vapor mass fraction distribution is shown in the Fig. 22, revealing that such cavitation is more likely to occur at the pump entrance (inlet) (Fig. 22).

The mass balance for the liquid phase is

$$\frac{\partial}{\partial t}(1-x_l)\rho_l + \nabla\left((1-x_l)\rho_l \vec{C}\right) = -\vec{R}. \tag{44}$$

The mass balance for the vapor phase is

$$\frac{\partial}{\partial t}x_v\rho_v + \nabla\left(x_v\rho_v \vec{C}\right) = \vec{R}. \tag{45}$$

The total energy mass balance is

$$\frac{\partial}{\partial t}\rho + \nabla\left(\rho \vec{C}\right) = 0. \tag{46}$$

In the case of a mixture of liquid and vapor, one has

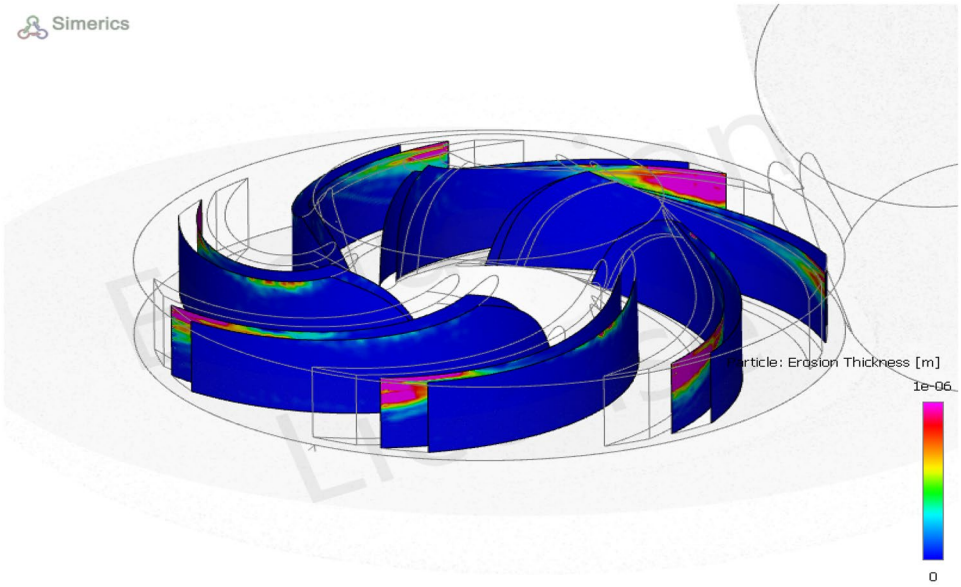

Fig. 26 Erosion thickness for $r = 10$ µm and density equal to 50 kg/m^3 (releasing mode: one time step)

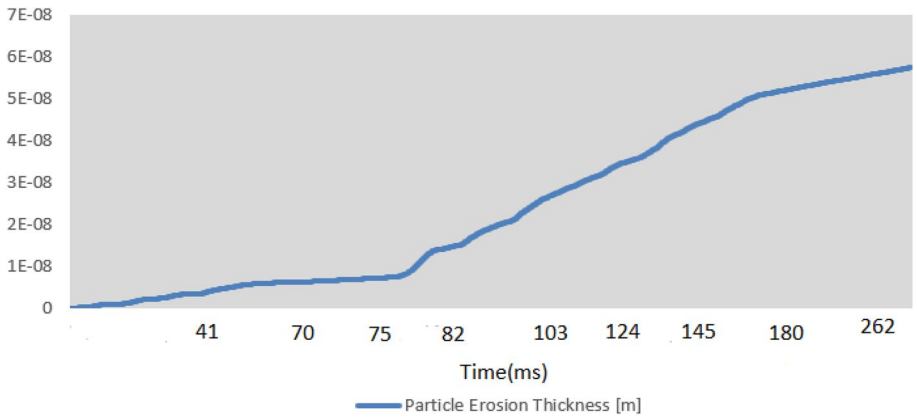

Fig. 27 Variation of the erosion thickness for a radial pump with time ($r = 10$ µm and density = 50 kg/m^3)

$$\rho = x_v \rho_v + \left(1 - x_v\right)\rho_l. \tag{47}$$

After combining Eqs. (44) and (43), we obtain

$$\nabla . \vec{C} = \frac{\rho_l - \rho_v}{\rho} \frac{\mathrm{d}x_v}{\mathrm{d}t}. \tag{48}$$

After simplification, this yields

$$R = \frac{\rho_v \rho_l}{\rho} \frac{\mathrm{d}x_v}{\mathrm{d}t}. \tag{49}$$

Finally, from Eq. (43), we have

$$\frac{\partial}{\partial t} x_v \rho_v + \nabla \left(x_v \rho_v \vec{C} \right) = \frac{\rho_v \rho_l}{\rho} \frac{\mathrm{d}x_v}{\mathrm{d}t}. \tag{50}$$

For the erosion rate simulation, the Finnie model was used with a velocity exponent of 2. The initial particle velocity was set to the fluid velocity, as we consider water to have a high density that will allow the particle to move with the fluid velocity. The particle radius was selected as 100 µm.

The particle trajectory was determined by using by Lagrange frame theory (Fig. 23).

The erosion rate depends on the release mode at the inlet section (Fig. 24). For this study, the mode with release every time step was selected.

The erosion weight is very high at the TE, where the absolute velocity is high. The variation of the erosion rate with time is shown in the next Figs. 25, 26.

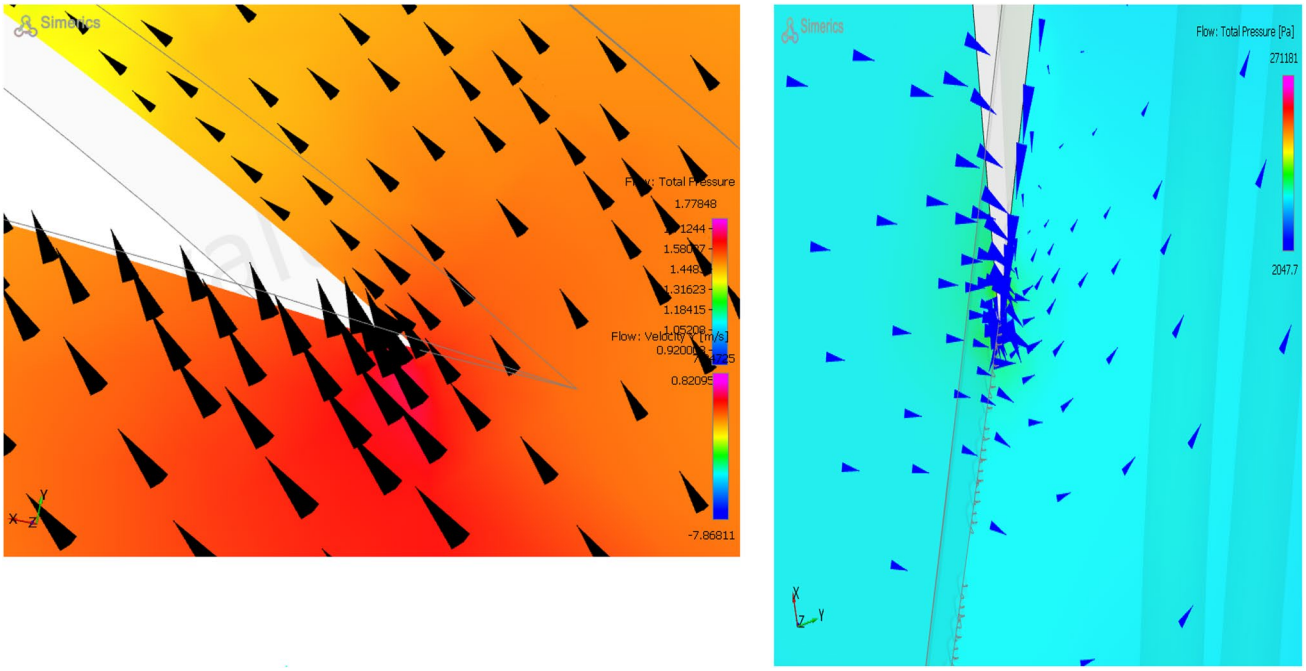

Fig. 28 The effect of the erosion on the flow stability for the design point (left side) and with 10% thickness loss (right)

For the simulation, we assume that, in each time step, we have the same number of particles injected in the same face at the entrance of the pump. As seen from Fig. 27, the thickness loss is linear with exposure time.

$$t_l = a \times t. \tag{51}$$

Th constant a depends on the material density, particle density, and erosion speed as

$$a = \frac{\rho_{\mathrm{p}} V_{\mathrm{erosion}}}{\rho_{\mathrm{m}}}. \tag{52}$$

In our case, the density of the particle is 998 kg/m^3, and $\rho_{\mathrm{m}} = 700$ kg/m^3, while the erosion velocity is equal to 0.02 m/s. This velocity will depend on the dimensionless parameters of the turbine, especially the specific speed.

The effect of the particle density results from the energy mass conservation:

$$\frac{4}{3}\pi {r_p}^3 \rho_p \frac{\mathrm{d}V_p}{\mathrm{d}t} = C_D {r_p}^2 \frac{\pi \rho_{sw} \left(V_p - C\right)^2}{2}. \tag{53}$$

If we assume

$$k = \frac{3}{8}\frac{\rho_w}{r_p \rho_p} C_{\mathrm{D}}, \tag{54}$$

$$\frac{V_p}{C} = \frac{k \cdot t V_p}{1 + k t V_p}. \tag{55}$$

The density ratio directly affects the particle velocity distribution owing to the drag forces. A high density means that V_{p} is equal to C. In this case, the erosion is dominated by the impingement angle.

The erosion velocity is reduced as the particle size or density is reduced. For this simulation, the release mode is one time step. The wall particle exhibits perfect bounce, and the release was from the center of the face.

From the graph below (Fig. 27), the erosion velocity is equal to 5×10^{-5} m/s.

After estimation of the thickness loss, one should consider the effect on flow stability. It was concluded that the loss of material mass can result in flow separation at the trailing edge of the pump (Fig. 28).

Conclusions and recommendations

Using seawater as a fluid for pumped storage systems can result in erosion and corrosion, especially on the turbomachinery side. For the Francis turbine runner, it was shown that the outlet radius and the inlet blade height have an impact on the velocity distribution. Increasing the outlet diameter may result in a reduction in the erosion rate,

whereas decreasing the blade height results in an increase in the inlet absolute velocity.

From the CFD analysis of a radial pump, it was concluded that the erosion thickness is high at the TE, where the absolute velocity of the fluid is important. A high erosion thickness causes flow separation, which implies an efficiency drop. The erosion velocity is proportional to the particle density and size (Fig. 28).

The flow separation is proportional to the blade thickness. In the case of seawater, the slip factor is affected by the corrosion. In this study, we concluded that a thickness loss of 10% due to erosion will induce flow deflection. For a good design, flow separation under 10% should be considered, as thickness loss is associated with the corrosion process.

Declarations

Conflict of interest On behalf of all authors, the corresponding author states that there is no conflict of interest.

References

Adnan Aslam Noon M-HK (2021) Sediment and cavitation erosion in Francis turbines—review of latest experimental and numerical techniques. Energies. https://doi.org/10.3390/en14061516

Aungier R (2000) Centrifugal compressors: a strategy for aerodynamic design and analysis. 2000 **(p. Chap 7)**.

Ayancik F (2014) Parametrical and theoretical design of a Francis turbine runner with the help of computational fluid dynamics. In: HEFAT2014 10th international conference on heat transfer, fluid mechanics and thermodynamics, 2014. https://doi.org/10.13140/2.1.3604.7683

Bardal E (1985) Korrosjon og korrosjonsvern

Biraj Singh Thapa BT, Dahlaug OG (2012) Empirical modelling of sediment erosion in Francis turbine. Energy. https://doi.org/10.1016/j.energy.2012.02.066

Dixon SL, Hall CA (2014) Chapter 9—hydraulic turbines. In: Dixon SL, Hall CA (eds) Fluid mechanics and thermodynamics of turbomachinery (seventh edition). Butterworth-Heinemann, Boston, pp 361–418

Finnie I (1960) Erosion of surfaces by solid particles. Wear 3(2):87–103. https://doi.org/10.1016/0043-1648(60)90055-7

Gautam S et al (2020) Sediment erosion in low specific speed Francis turbines: a case study on effects and causes. Wear 442–443:203152–203152. https://doi.org/10.1016/j.wear.2019.203152

Gülich JF (2014) Centrifugal pumps 7–10

Hashimoto T (1986) Seawater pumped storage scheme under study in Japan. International water power and dam construction

Koirala R et al (2016) Sediment erosion in guide vanes of Francis turbine: a case study of Kaligandaki hydropower plant, Nepal. Wear 362–363:53–60. https://doi.org/10.1016/j.wear.2016.05.013

Messa GV, Mandelli S, Malavasi S (2019) Hydro-abrasive erosion in Pelton turbine injectors: a numerical study. Renew Energy 130:474–488. https://doi.org/10.1016/j.renene.2018.06.064

Padhy MK, Saini RP (2011) Study of silt erosion on performance of a Pelton turbine. Energy 36(1):141–147. https://doi.org/10.1016/j.energy.2010.10.060

Sangal S, Singhal MK, Saini RP (2018) Hydro-abrasive erosion in hydro turbines: a review. Int J Green Energy 15(4):232–253. https://doi.org/10.1080/15435075.2018.1431546

Schwanse M (1990) Strömungsmechanische Auslegung und Nachrechnung von radialen und diagonalen Kreiselpumpenlaufrädern (in German). Dissertation, 1990, pp 60–70